Applied & Translational Genomics 7 (2015) 2–12

Contents lists available at ScienceDirect

Applied & Translational Genomics

journal homepage: www.elsevier.com/locate/atg

Identification and conformational analysis of putative microRNAs in *Maruca vitrata* (Lepidoptera: Pyralidae)

C. Shruthi Sureshan, S.K.M. Habeeb *

Department of Bioinformatics, School of Bioengineering, SRM University, Kattankulathur 603203, Tamil Nadu, India

ARTICLE INFO

Article history:
Received 14 May 2015
Received in revised form 21 August 2015
Accepted 14 October 2015

Keywords:
MicroRNA
Maruca vitrata
Transcriptome
Precursor microRNA
Torsion angle

ABSTRACT

MicroRNAs (miRNAs) are a class of small RNAs, evolutionarily conserved endogenous non-coding RNAs that regulate their target mRNA expression by either inactivating or degrading mRNA genes; thus playing an important role in the growth and development of an organism. *Maruca vitrata* is an insect pest of leguminous plants like pigeon pea, cowpea and mung bean and is pantropical. In this study, we perform BLAST on all known miRNAs against the transcriptome data of *M. vitrata* and thirteen miRNAs were identified. These miRNAs were characterised and their target genes were identified using TargetScan and were functionally annotated using FlyBase. The importance of the structure of pre-miRNA in the Drosha activity led to study the backbone torsion angles of predicted pre-miRNAs (mvi-miR-9751, mvi-miR-649-3p, mvi-miR-4057 and mvi-miR-1271) to identify various nucleotide triplets that contribute to the variation of torsion angle values at various structural motifs of a pre-miRNA.

1. Introduction

Insect infestation on a crop leads to loss in yield and quality, and then the insect becomes agricultural pest. The legume pod borer, *Maruca vitrata* (lepidopteran) is one of the serious pest of grain legumes in the tropics and sub-tropics (Sharma, 1998); and they are known to affect overall production by causing damage to pigeon pea (Gopali et al., 2010), mung bean (Zahid et al., 2008) and cowpea (Asante et al., 2001). In Bangladesh, the damage caused by pod borer was estimated to be 54.4% in cowpea during harvest (K. O and M.Z. A., 1989). Reports from Taiwan show a yield loss of 17–53% of cowpea due to the pod borer infestation (Liao and Lin, 2000). Larvae web around the leaves and inflorescence before boring, and this prevents the pesticide penetration into the larval nest. Hence, control of this pest becomes challenging and there is a need for better control measures and strategies. Identification of various entomopathogenic fungus and parasitoids associated with *M. vitrata* is an effective method to kill or disable the insect (Mehinto et al., 2014; Dannon et al., 2010). Artificial miRNAs (amiRNAs) mediated gene silencing is turning into a potent tool in functional genomics, to control gene expression. They can be further utilized to study metabolic pathway and gene functions in various disciplines, and even to enhance favourable traits in plants (Tiwari et al., 2014; Cantó-Pastor et al., 2015).

MicroRNAs (miRNAs) are a class of ~21 nt, endogenous non-coding RNA, that regulate target mRNA by cleaving or translation repression (Bartel, 2004). They play significant roles like developmental timing, cell differentiation and proliferation, tumorigenesis, host–pathogen interactions, ageing and viral replication (Ambros, 2012; Shivdasani, 2006; Gong et al., 2012; Asgari, 2011; Drummond et al., 2011). The structure of a pri-miRNA consists of a long imperfect stem structure of ~30 bp with flanking single-stranded RNA segments at its base. Maturation of miRNA begins when pri-miRNA is cleaved with an RNase enzyme III named Drosha (Lee et al., 2003) to release an ~60–70 nucleotide stem-loop intermediate known as the precursor miRNA (pre-miRNA). The pre-miRNA is transported to cytoplasm where RNase III enzyme called Dicer cleaves it to generate mature miRNA (Flores-jasso et al., 2009). The incorporation of the mature miRNA (guide strand) into the RNA induced silencing complex (RISC) triggers the recognition of target mRNA and inactivates or degrades it.

Stem-loop hairpin structure is an important feature of pre-miRNA in the computational identification of miRNA genes and in the biogenesis of miRNA (Krol and Krzyzosiak, 2004). The variation in the length of mature miRNA depends on the manner the enzyme Dicer cleaves the pre-miRNA, which in turn depends on the structural motifs like terminal loops, internal loops, and bulges present in the pre-miRNA. Terminal loop plays a major role in the cleaving action of Drosha and Dicer on the pre-miRNA (Starega-Roslan et al., 2011). As *M. vitrata* is an important pest, identifying miRNAs present in this lepidopteran will be practical in order to mediate gene silencing and transgenesis studies.

Torsion angle is a critical factor to be analysed while examining various DNA/RNA motifs and conformations. The conformation of the backbone of DNA/RNA is defined by torsion angles — α, β, γ, δ, ε, and ζ. And the orientation of a base relative to sugar is given by torsion

* Corresponding author.
E-mail address: habeeb_skm@yahoo.co.in (S.K.M. Habeeb).

http://dx.doi.org/10.1016/j.atg.2015.10.003

angle χ and there is a correlation between the angles — α↔γ and ε↔ζ (Saenger, 1983). The torsion angle studies had been applied to DNA Holliday Junction structure (Eichman et al., 2002), α/γ transitions in B-DNA backbone (Djuranovic et al., 2002), conformational classification of RNA (Schneider et al., 2004) and structural modifications in histones (Sanli et al., 2011). Analysis of torsion angles determines the irregularities in a structure. Every backbone torsion angle consists of certain range of values that maintains the integrity of the structure. Deviation from these values distorts the structure and hence its function (Temiz et al., 2012). In this study, we have investigated the fluctuations imposed on torsion angles with the variations observed in the sequence of miRNAs (Svozil et al., 2008).

Existing transcriptome data were used to identify and characterise the putative miRNAs in *M. vitrata*; in order to predict target genes for the predicted miRNA and functionally annotate them using TargetScan and FlyBase respectively; and also to study the sequence dependant variations in backbone torsion angles in predicted miRNAs.

2. Materials and method

2.1. Data collection and identification of putative miRNA and their precursor

The transcriptome data of *M. vitrata* was retrieved from Sequence Read Archive, NCBI. The complete collection of miRNAs was downloaded from miRBase (Griffiths-Jones et al., 2006). The transcriptome data was processed to generate contigs and remove redundant sequences, and only the non-homologue sequences were used for further analysis.

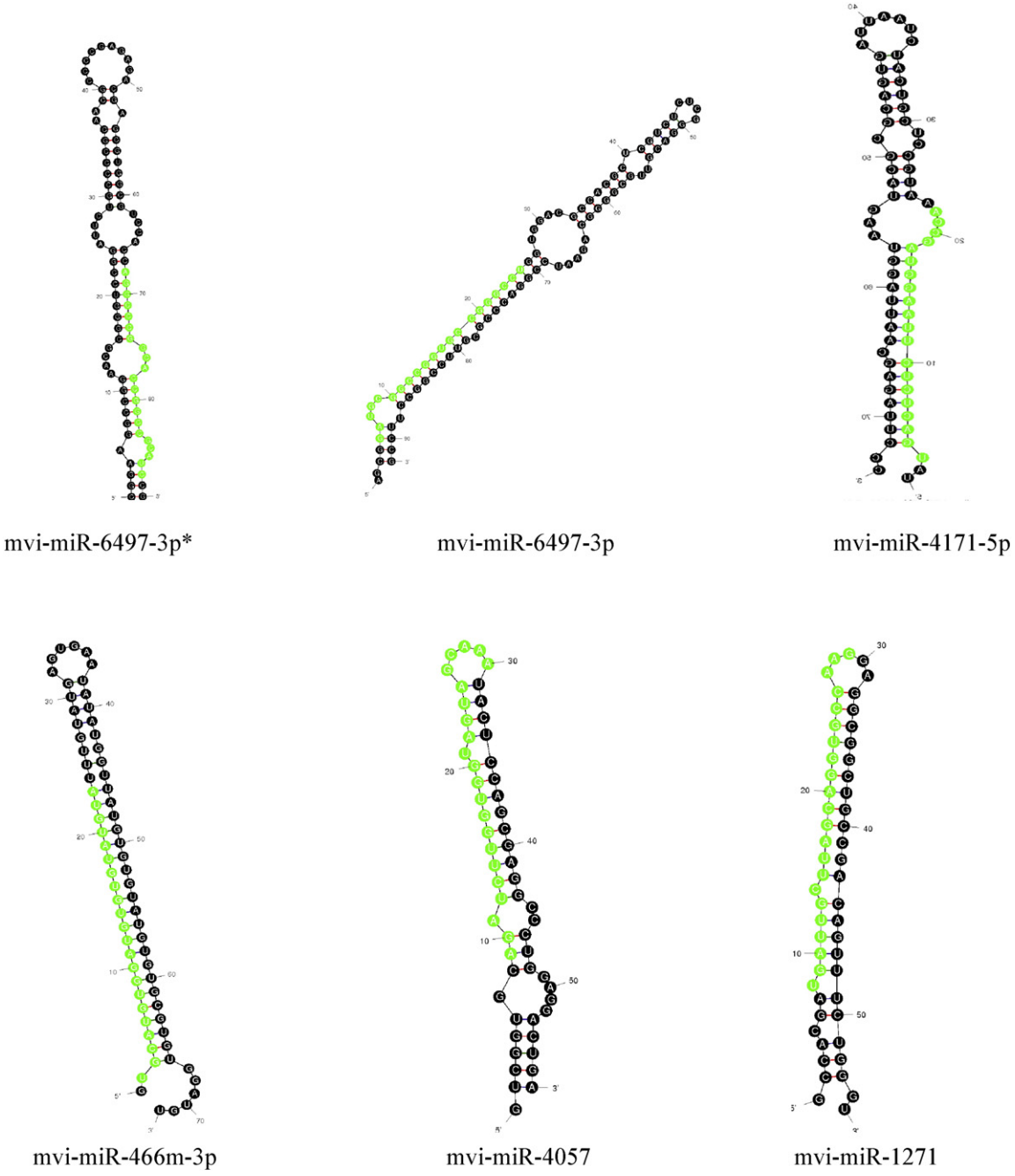

Fig. 1. The secondary structures of putative miRNAs: The secondary structure consists of a stem and loop structures. The highlighted regions represent the mature microRNA in the hairpin structure.

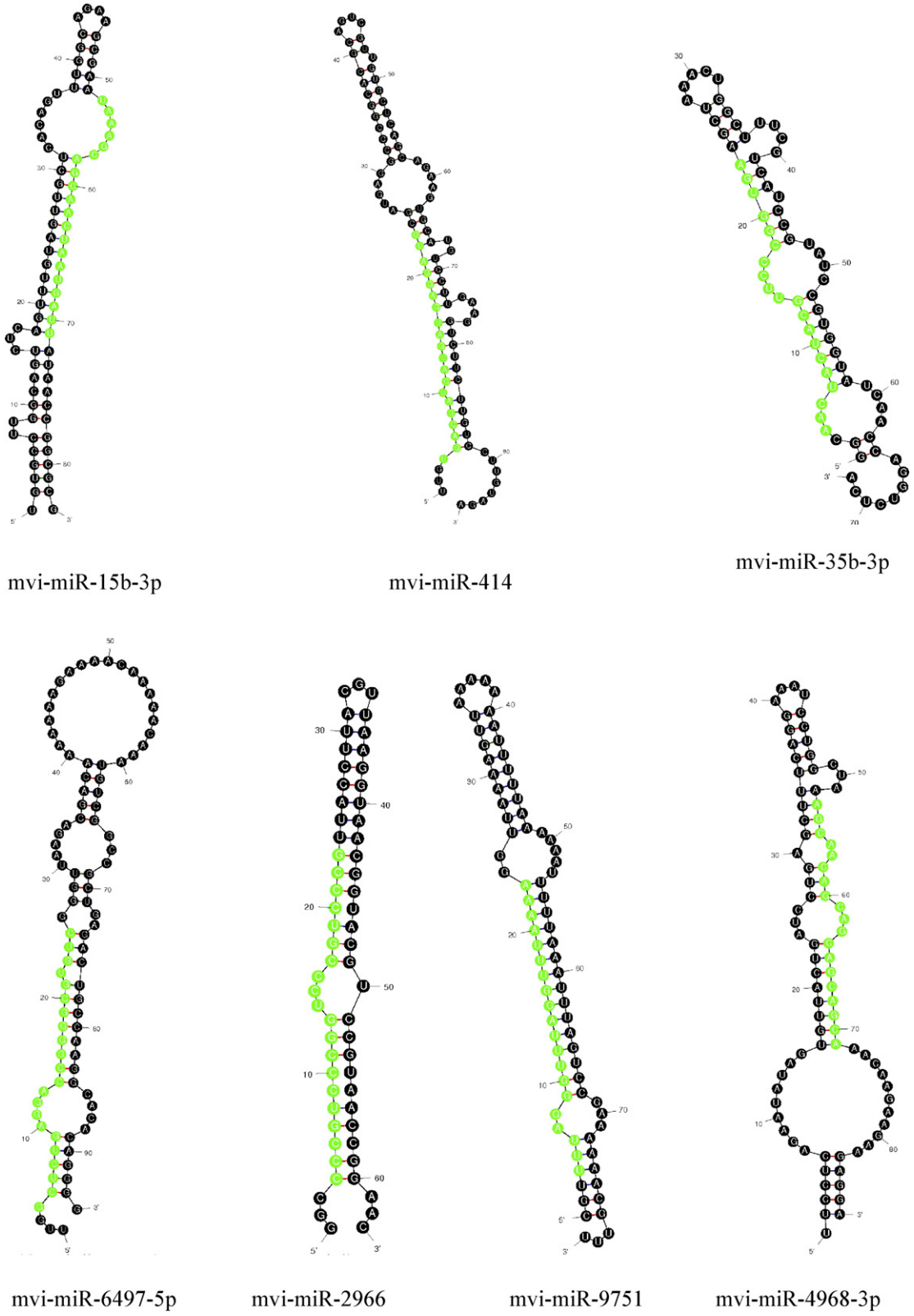

Fig. 1 (*continued*).

The collected miRNA sequences were used as query for homologous search against the transcriptome data, using standalone BLAST +2.2.28 programme (Altschul et al., 1997).The hits obtained were considered as the candidates for finding precursor miRNAs. These sequences were submitted to Mfold to predict the secondary structures of precursor miRNAs (Zuker, 2003). The secondary structures were predicted based on criteria determined by Zhang et al. (2006):

1. The pre-miRNA could be able to fold into a typical hairpin secondary structure.

2. The mature miRNA should be located in the stem region of the hairpin structure.
3. miRNA has less than seven mismatches with the complementary sequence in the opposite arm.
4. No loops or breaks are allowed in the miRNA or miRNA*duplex.
5. The negative MFE of the miRNA should be greater than −18 kcal/mol and the (A + U) content must be in the range of 40–70%.

The predicted miRNAs were named in accordance with the rules determined in the miRBase (Griffiths-Jones et al., 2006).

2.2. Predicting targets of miRNA

The target genes of the predicted miRNAs were identified using TargetScan (Lewis et al., 2003). TargetScan predict targets of miRNAs by searching for the presence of conserved sites that match the seed region of miRNA. The target genes obtained are then directed to the FlyBase database (Dos Santos et al., 2014), which assist in the functional annotation.

2.3. Predicting three dimensional structure of miRNA and torsion angle analysis

The three dimensional structure of mvi-miR-9751, mvi-miR-6497-3p, mvi-miR-4057 and mvi-miR-1271was constructed using MC-Sym (Parisien and Major, 2008), which provides a fully automated 3D structure from the user defined secondary structure (in Vienna format) and the sequence of microRNA in study. The PDB files created for the four predicted miRNAs were used to generate the torsion angle data using Curves + (Lavery et al., 2009). Graphs were generated to analyse torsion angle data (.lis file).

3. Results and discussion

In this study, 13 miRNAs were identified in the insect *M. vitrata* from the transcriptome data.

3.1. Characterisation of miRNA

All the predicted miRNAs have a typical stem-loop structure. The mature miRNAs were located either in 5′ arm (62%) or the 3′ arm (38%) of the stem loop structure. The secondary structures of all the predicted miRNAs are given in Fig. 1.

The length of mature miRNAs varies from 19 to 22 nucleotides and the length of pre-miRNAs varied from 55 to 96 nucleotides. Tables 1 and 2 show the details of precursor miRNAs and predicted mature miRNAs respectively.

Minimum free energy (MFE) calculated for the predicted miRNAs varied from −51.2 to −16 kcal/mol (Das, 2010). The A + U content for the predicted pre-miRNA varied from 24 to 80% (Asokan et al., 2013).

3.2. Identification of miRNA targets

In animals, the miRNA and microRNA Response Element (MRE) are almost never completely complementary to each other. The “seed” region which constitutes roughly 6–8 nucleotides of the 5′-end generally suffices the functional RISC formation (Brennecke et al., 2005). But recent

Table 1
Details of predicted precursor miRNAs.

miRNA	miRNA sequence	MFE	E value	A + U content
mvi-miR-6497-3p*	CGGAAGGCCGGAACGCGGGUCCGGAUUCU GCCCCGCAACGCCCCGAGAGACGAGCGUGG CGUCCACCAGGCCCGGCACCGGCCGCAUCCG	−38.5	0.001	24.44
mvi-miR-6497-3p	AGCGGAUGCGGCCGGUGCCGGGCCUGGUGG ACGCCACGCUCGUCUCUCGGGACGUUGCGGG GCAGAAUCCGGACCCGCGUUCCGGCCUUCCG	−51.2	0.001	26.08
mvi-miR-4171-5p	UAUGACUCUCUUAAGGUAGCCAAAUGCCUC GUCAUCUAAUUAGUGACGCGCAUGAAUGGA UUAACGAGAUUCCC	−16.7	0.003	56.75
mvi-miR-466m-3p	GUGCAUGUGGAUGUGUGUAUGUAUUUGUA UGAGUGAAUAUAUGGUUAUGUGUGUAUGU GUGCGUGUGGAUGU	−19.4	0.004	61.11
mvi-miR-4057	GUCGGUGCAGAUCUUGGUGGUAGUAGCAAA UACUCCAGCGAGGCCCUGGAGGACUGA	−17.9	0.004	43.85
mvi-miR-1271	GCCACGAUGAUUGCUUAGCAGGUGCCAAGG AGGCGGCUGCCGACAGUUUCUGGGU	−21.7	0.004	40
mvi-miR-15b-3p	UGUGCCUUGGCAGUCUCAGUUUGUAGUUGC UCACAGUUUGGCAGAAGCGAAUAAAGCAG CAACUAAUGAUUAUAACCGGCGCG	−20.8	0.004	53.01
mvi-miR-414	UUGUGACGAUGAUGAUGAGGAUGCGAUGA GGCCCGGCACGCAGUCGUUGUGCUCAGCA GAAGUGCAUGUCCUUGAAGGUCUUCUUGU CCUUGUAGA	−25.4	0.004	47.91
mvi-miR-35b-3p	GGCAACUACUACGUUCCCGGUGAAGCUAA ACUGGCUUUCGUCAUCCGUAUCCGUGGUA UCAACCAGGUCUCA	−17.4	0.004	48.61
mvi-miR-6497-5p	UUGGCUCUGAGGACCGGGGCGUGUCGGGU UAAGACGACAAAAAAAGAAAACAAAAACA AAUGUCGGCCGCUGAGACUGCCAAGGCAC ACAGGGG	−24.2	2.00E−05	46.8
mvi-miR-2966	GGCCCCGUCCCGGUCCCGUCCCGUUACCUUAC GUUAAGGUAACGGUACGUCCGUAACCGGAAC	−26.3	2.00E−04	38.09
mvi-miR-9751	CGUUUUAGGGUUUAGGUUUAAAAGGUUAAA AGUUAAAAAAAUUUUUAAAAAAUUUUUAAA UUUAGUCCGAAAAAACGUUU	−16	4.00E−04	80
mvi-miR-4968-3p	UUCCUCAGAAUAUAGUGUUACUGAUCCUGA GCUUUCAGGAAAUCCUGGCUAAAGCAACAG CAGCAGCAGCAAACAAGAAGAAGAGGA	−22.8	8.00E−04	56.32

Table 2
Details of predicted mature miRNAs.

miRNA	Contig/singlet	Start position	End position	Strand	miRNA sequence
mvi-miR-6497-3p*	1768	475	495	3′	AGGCCCGGCACCGGCCGCAUC
mvi-miR-6497-3p	524	133	153	5′	GAUGCGGCCGGUGCCGGGCCU
mvi-miR-4171-5p	5676	3	22	5′	UGACUCUCUUAAGGUAGCCA
mvi-miR-466m-3p	5130	450	471	5′	UACAUACACACAUCCACAUGCA
mvi-miR-4057	4013	332	311	5′	UUUGCUACUACCACCAAGAUCU
mvi-miR-1271	971	568	547	5′	CUUGGCACCUGCUAAGCAAUCA
mvi-miR-15b-3p	5346	93	74	3′	AAUCAUUAGUUGCUGCUUUA
mvi-miR-414	3442	746	727	5′	CAUCCUCAUCAUCAUCGUCA
mvi-miR-35b-3p	4714	347	328	5′	UCACCGGGAACGUAGUAGUU
mvi-miR-6497-5p	FTWC1V114IJAVH	367	388	5′	GCUCUGAGGACCGGGGCGUGUC
mvi-miR-2966	FTWC1V113H8JH6	570	551	5′	CCCGUCCCGGUCCCGUCCCG
mvi-miR-9751	FTWC1V112HKXA0	290	271	5′	UUUUAAACCUAAACCCUAAA
mvi-miR-4968-3p	FTWC1V116JP5XD	161	179	3′	AGCAACAGCAGCAGCAGCA

studies prove that seed target regions at the 3′-end are conserved and thus demonstrating the predominant regulatory functions of miRNAs through 3′ UTRs (Gu et al., 2007; Friedman et al., 2009). In the current study, we have used 3′ UTR sequence data of *Drosophila melanogaster* in the TargetScan to confirm our targets (Table 3).

3.3. Functional annotation

A total of 141 targets were obtained for 13 miRNAs encoding for metamorphosis, cell signalling, transcription regulation, structural constituents, metabolism, and transmembrane transportation. Thus it proves the multi-level functioning of miRNAs in various molecular and cellular processes.

mRNAs targeted by mvi-miR-466m-3p and mvi-miR-1271 are associated with Hedgehog receptor activity and Ecdysis-triggering hormone receptor activity which are linked to metamorphosis. mvi-miR-9751 was seen to target genes mainly associated with transcription regulation, which is accomplished by sequence specific DNA binding proteins, RNA polymerase II transcription cofactor and histone methyltransferase activity. Further, mvi-miR-9751 also controlled the genes specific to GTPase activity and serotonin activity, which are integral to various signalling pathways. Similarly mvi-miR-4968-3p was found to be associated with transcription regulating proteins as well as signalling molecules (Ras GTPase binding).

mvi-miR-6497-3p* targets mRNAs linked to structural constituents of chorion (the outer shell of the insect egg) along with the protein serine/threonine phosphatase activity. Apart from mvi-miR-6497-3p*, structural constituents of chorion are also targeted by mvi-miR-414 and mvi-miR-35b-3p. mvi-miR-1271 and mvi-miR-4968-3p regulate the genes related to structural constituents of cytoskeleton.

3.4. Target multiplicity and cooperativity

Multiplicity is one of the common characteristics of miRNA regulation, such that one 3′ UTR has more than one MREs and thus assisting miRNA in having multiple targets (Ghosh et al., 2007). In our study we identified mvi-miR-9751 to have maximum plausible target mRNAs responsible for transcription regulation and signalling pathways.

Cooperativity is another feature shown by miRNA, where more than one miRNAs regulate a target mRNA, thus establishing an effective silencing (Ghosh et al., 2007). In our study we found that mvi-miR-6497-3p* and mvi-miR-35b-3p participate in the regulation of the gene FBgn0000359 (structure of chorion).

3.5. Torsion angle analysis

In order to study the fluctuations observed in torsion angle with respect to the variation in sequences, the structure of mvi-miR-9751 was divided into one loop, three stem sections and one internal loop. Similarly, one loop, five stem sections, one bulge and one internal loop in mvi-miR-649-3p; two stem sections and one internal loop for mvi-miR-4057; one external loop, two stem sections, one bulge and one loop for mvi-miR-1271 were noted down for the analysis. The four torsion angles, α, γ, ε and ζ have shown deviation from their usual range of values. Similar to DNA sequences, miRNA has relationship between the torsion angles (Saenger, 1983):

1. Alpha (α) and gamma (γ)
2. Epsilon (ε) and zeta (ζ).

Figs. 2, 3, 4, 5 shows the relationships and deviations observed in the torsion angles in mvi-miR-9751, mvi-miR-649-3p, mvi-miR-4057 and mvi-miR-1271 respectively. Tables 4 and 5 shows the maximum and minimum values of α, γ, ε and ζ torsion angles in the stems, loops, internal loops and bulge regions of the two miRNAs.

3.5.1. Deviation of alpha and gamma torsion angles

In general the values of α torsion angles for RNA is specific to the *−gauche* region (−30° to −90°) of the Klyne and Prelog cycle. Most of the nucleotides have been found to be in this region, with few exceptions. There were deviations from the *−sc* to *−ac*, *−ap*, *+ap*, *+ac* and *+sc* regions. Majority of them were found to be in *−ac* and *−ap* regions. For the most part, this variation has been observed in nucleotides — C and G.

The usual range of γ torsion angles for RNA is *+gauche* (30° to 90°) of the Klyne and Prelog cycle. All the four microRNA sequences have shown a predominant deviation to *+ac*, *−ac*, *−ap* and *+ap* regions. Overall, both α and γ values were found to be in similar ranges with respect to various studies (Schneider et al., 2004).

3.5.2. Deviation of epsilon and zeta torsion angles

The normal range of ϵ torsion angle has been mainly recorded to be in the *−ac* (−90° to −150°) region (Schneider et al., 2004). But apart from this region, the *+ap* and *−sc* regions are also allowed if the ribose sugar exhibits $C_{3'}$ endo- and $C_{3'}$ exo-puckering respectively. It was noted that most of the nucleotides in our miRNAs had ϵ torsion angles that have occupied a different region other than *−ac*. The epsilon values have shifted to the *−ap* and *+sc* regions. As a result of $C_{3'}$ endo-puckering, G_{43} (mvi-miR-4051), G_{50} and U_{56} (mvi-miR-6497-3p) displayed values in the *−sc* region, similarly, due to $C_{3'}$ exo-puckering C_5 of mvi-miR-1271 showed values in the *+ap* region.

The ζ values are generally depicted in the *−gauche* (−30° to −90°) region and some cases to the *−ap* region too. Our study showed deviations from this range of values in some of the nucleotides. The torsion angle mostly shifted to *−ac* and *+ac*, and a few were found to be in *+sp* and *−sp* regions.

Table 3
Target mRNAs for the predicted miRNAs and their functional annotations.

miRNA	Target gene	Symbol	Function
mvi-miR-6497-3p*	FBgn0035746	CG17742	Identical protein binding
	FBgn0000359	CG1478	Structural constituent of chorion
	FBgn0004177	CG7109	Protein serine/threonine phosphatase activity
mvi-miR-6497-3p	FBgn0034100	CG15709	Intracellular cyclic nucleotide activated cation channel activity
	FBgn0013733	CG18076	Protein binding
mvi-miR-4171-5p	FBgn0003031	CG5119	mRNA 3′-UTR binding
	FBgn0010452	CG11280	Unknown
	FBgn0033989	CG7639	Unknown
mvi-miR-466m-3p	FBgn0013974	CG42636	Guanylate cyclase activity
	FBgn0003892	CG2411	Hedgehog receptor activity
	FBgn0020245	CG10117	Protein binding
	FBgn0024277	CG18214	Rho guanyl-nucleotide exchange factor activity
	FBgn0034451	CG11242	Unknown
	FBgn0000036	CG5610	Acetylcholine-activated cation-selective channel activity
	FBgn0000037	mAcR-60C	G-protein coupled acetylcholine receptor activity
	FBgn0000439	CG2189	Activating transcription factor binding
	FBgn0001122	CG2204	GTP binding
mvi-miR-4057	FBgn0000286	CG11924	DNA binding
	FBgn0033494	CG33135	Voltage-gated cation channel activity
	FBgn0000497	CG17941	Cadherin binding; calcium ion binding
	FBgn0003380	CG12348	Voltage-gated cation channel activity
	FBgn0003520	CG5753	mRNA 3′-UTR binding
	FBgn0004198	CG11387	Transcription regulatory region sequence-specific DNA binding
	FBgn0004889	CG6235	Protein phosphatase type 2A regulator activity
	FBgn0005638	CG4354	RNA polymerase II regulatory region sequence-specific DNA binding
	FBgn0010453	CG4698	Frizzled binding
	FBgn0013342	CG17248	Protein binding; SNAP receptor activity; SNARE binding
	FBgn0015286	CG2849	GTPase activity; PDZ domain binding
	FBgn0015797	CG6601	GTPase activity
	FBgn0022131	CG42783	Myosin binding; protein serine/threonine kinase activity
	FBgn0026616	CG4606	Mannosyl-oligosaccharide 1,2-alpha-mannosidase activity
	FBgn0034476	CG8595	Neurotrophin receptor activity; virion binding
	FBgn0035167	CG13888	Sweet taste receptor activity
	FBgn0035895	CG7015	mRNA 3′-UTR binding
	FBgn0036862	CG9619	Protein phosphatase 1 binding
	FBgn0038587	CG7998	Malate dehydrogenase activity
	FBgn0039054	CG13830	Wnt-protein binding
	FBgn0041092	CG13109	Ligand-dependent nuclear receptor transcription coactivator activity; steroid hormone receptor binding
mvi-miR-1271	FBgn0052062	CG32062	Transcription factor binding
	FBgn0011674	CG11312	Cytoskeletal adaptor activity
	FBgn0038165	CG9637	Potassium channel activity; protein heterodimerization activity
	FBgn0000119	CG5912	Wnt-activated receptor activity
	FBgn0053517	CG33517	Dopamine neurotransmitter receptor activity
	FBgn0038874	CG5911	Ecdysis-triggering hormone receptor activity
	FBgn0038818	CG4058	Metalloendopeptidase activity
	FBgn0004370	CG1817	Protein tyrosine phosphatase activity
	FBgn0004514	CG7485	G-protein coupled amine receptor activity
	FBgn0024273	CG1520	Actin binding
mvi-miR-15b-3p	FBgn0001145	CG1743	Glutamate-ammonia ligase activity
	FBgn0026375	CG32555	Rho GTPase activator activity; semaphorin receptor binding
	FBgn0086783	CG17927	Actin-dependent ATPase activity; protein homodimerization activity; structural constituent of muscle
	FBgn0001085	CG17697	Wnt-activated receptor activity
	FBgn0001235	CG17117	Sequence-specific DNA binding transcription factor activity
	FBgn0003525	CG1395	Protein tyrosine phosphatase activity
	FBgn0036757	CG14585	Extracellular ligand-gated ion channel activity; olfactory receptor activity
	FBgn0003502	CG8049	Protein tyrosine kinase activity
	FBgn0003710	CG1232	Sodium channel regulator activity
	FBgn0004103	CG5650	Myosin phosphatase activity; protein serine/threonine phosphatase activity
	FBgn0004598	CG18734	Serine-type endopeptidase activity
	FBgn0263111	CG43368	Voltage-gated calcium channel activity
	FBgn0010453	CG4698	Frizzled binding
	FBgn0013995	CG5685	Calcium:sodium antiporter activity
	FBgn0015797	CG6601	GTPase activity
	FBgn0030366	CG1490	Ubiquitin-specific protease activity
mvi-miR-414	FBgn0000359	CG1478	Structural constituent of chorion
	FBgn0021764	CG5227	Unknown
mvi-miR-35b-3p	FBgn0000360	CG11213	Structural constituent of chorion
	FBgn0039674	CG1907	Oxoglutarate:malate antiporter activity; transmembrane transporter activity
	FBgn0250910	CG42244	Octopamine receptor activity
mvi-miR-6497-5p	FBgn0004636	CG1956	GTPase activity
	FBgn0031530	CG3254	Polypeptide N-acetylgalactosaminyltransferase activity
mvi-miR-2966	FBgn0025625	CG4290	Protein kinase activity
	FBgn0032419	CG17217	Unknown
mvi-miR-9751	FBgn0003415	CG9936	RNA polymerase II transcription cofactor activity
	FBgn0037351	CG1475	Structural constituent of ribosome

(continued on next page)

Table 3 (*continued*)

miRNA	Target gene	Symbol	Function
mvi-miR-9751	FBgn0037834	CG6554	Histone methyltransferase activity (H4-R3 specific); protein-arginine omega-N asymmetric methyltransferase activity
	FBgn0000448	CG33183	Ligand-activated sequence-specific DNA binding RNA polymerase II transcription factor activity; protein binding
	FBgn0015806	CG10539	Ribosomal protein S6 kinase activity
	FBgn0032480	CG5682	Unfolded protein binding
	FBgn0063499	CG17522	Glutathione transferase activity
	FBgn0010280	CG5444	RNA polymerase II core promoter sequence-specific DNA binding transcription factor activity involved in preinitiation complex assembly
	FBgn0041092	CG13109	Ligand-dependent nuclear receptor transcription coactivator activity; steroid hormone receptor binding
	FBgn0000097	CG3166	Protein binding; RNA polymerase II distal enhancer sequence-specific DNA binding transcription factor activity
	FBgn0000247	CG31037	Rab GTPase binding; Rab guanyl-nucleotide exchange factor activity
	FBgn0000253	CG8472	Calcium ion binding; myosin heavy chain binding; myosin V binding
	FBgn0000283	CG6384	Chromatin insulator sequence binding; DNA binding; microtubule binding; POZ domain binding;
	FBgn0003137	CG33103	Extracellular matrix structural constituent
	FBgn0003410	CG9949	Protein binding; protein self-association
	FBgn0003892	CG2411	Hedgehog receptor activity; lipoprotein particle receptor activity
	FBgn0003944	CG10388	DNA binding; protein binding; protein domain specific binding; RNA polymerase II distal enhancer sequence-specific DNA binding
	FBgn0004168	CG16720	Serotonin receptor activity
	FBgn0004242	CG3139	Calcium-dependent phospholipid binding; phosphatidylserine binding; protein homodimerization activity; SNARE binding
	FBgn0005631	CG13521	Heparin binding; protein binding
	FBgn0011217	CG7425	Ubiquitin conjugating enzyme activity; ubiquitin protein ligase activity; ubiquitin protein ligase binding
	FBgn0015790	CG5771	GTPase activity; protein binding; protein complex binding
	FBgn0262872	CG43227	Myosin binding
	FBgn0026391	CG16961	Olfactory receptor activity
	FBgn0028875	CG32975	Acetylcholine binding
	FBgn0028996	CG1922	RNA polymerase II core promoter proximal region sequence-specific DNA binding transcription factor activity involved in positive regulation of transcription
	FBgn0264386	CG15899	Low voltage-gated calcium channel activity
	FBgn0034691	CG6562	Inositol-polyphosphate 5-phosphatase activity
	FBgn0036373	CG10741	Transcription coactivator binding; transcription factor binding
	FBgn0037950	CG14723	Histamine-gated chloride channel activity
	FBgn0001233	CG1242	Unfolded protein binding
	FBgn0002917	CG1517	Cation channel activity
	FBgn0261606	CG15442	Structural constituent of ribosome
	FBgn0011224	CG31000	mRNA 3′-UTR binding; translation repressor activity, nucleic acid binding
	FBgn0011225	CG5695	Actin binding; actin filament binding; calmodulin binding; microtubule binding; myosin light chain binding
	FBgn0013467	CG18285	Calmodulin binding
mvi-miR-4968-3p	FBgn0001122	CG2204	GTP binding
	FBgn0003721	CG4898	Actin filament binding
	FBgn0011656	CG1429	RNA polymerase II core promoter proximal region sequence-specific DNA binding transcription factor activity involved in positive regulation of transcription
	FBgn0259162	CG42267	ATP binding
	FBgn0042083	CG3267	CoA carboxylase activity
	FBgn0259227	CG42327	Protein tyrosine phosphatase activity
	FBgn0002441	CG5954	Chromatin insulator sequence binding
	FBgn0002932	CG11988	Phosphatidylinositol phosphate binding; protein binding; ubiquitin protein ligase activity
	FBgn0261873	CG32717	Protein binding
	FBgn0004364	CG8896	Transmembrane signalling receptor activity
	FBgn0003423	CG1417	Proline dehydrogenase activity
	FBgn0004636	CG1956	GTPase activity; protein binding
	FBgn0010516	CG8996	Electron carrier activity; flavin adenine dinucleotide binding
	FBgn0264855	CG4260	Protein transporter activity
	FBgn0020309	CG14938	Metal ion binding; nucleic acid binding
	FBgn0027844	CG7820	Carbonate dehydratase activity; zinc ion binding
	FBgn0031432	CG9964	Electron carrier activity
	FBgn0264815	CG44007	3′,5′-Cyclic-AMP phosphodiesterase activity
	FBgn0033095	CG3409	Monocarboxylic acid transmembrane transporter activity
	FBgn0033317	CG8635	Metal ion binding
	FBgn0033460	CG1472	Signal sequence binding; transporter activity; zinc ion binding
	FBgn0033609	CG13213	SAM domain binding
	FBgn0034967	CG3186	Ribosome binding
	FBgn0035357	CG1244	Chromatin binding; nucleosome-dependent ATPase activity; protein binding
	FBgn0035914	CG6282	Oxidoreductase activity, acting on the CH-CH group of donors
	FBgn0036005	CG3428	Contributes to ubiquitin–protein transferase activity
	FBgn0036816	CG3979	Citrate transmembrane transporter activity; succinate transmembrane transporter activity
	FBgn0050286	CG30286	Serine-type endopeptidase activity
	FBgn0259176	CG42281	Protein homodimerization activity; sequence-specific DNA binding transcription factor activity
	FBgn0038153	CG14376	Ligand-gated ion channel activity
	FBgn0052654	CG32654	Ras GTPase binding

3.5.3. Nucleotides showing deviation in torsion angles

The torsion angle values under the study have shown to deviate with respect to changes in nucleotide sequence (Svozil et al., 2008). Among all the four nucleotide, G and C have induced the most deviation in torsion angle (Arrigo et al., 2012). The values of torsion angles fluctuated with respect to certain patterns of nucleotide

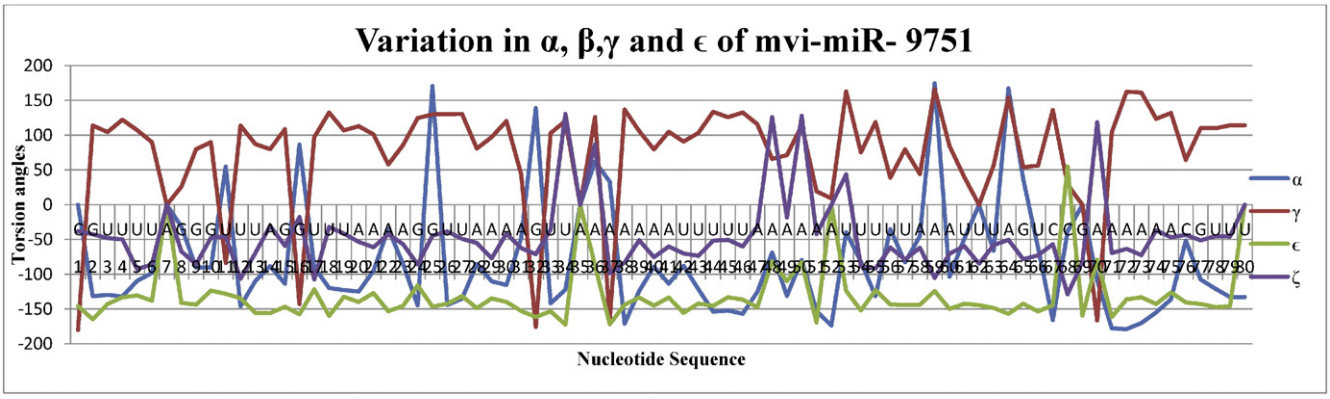

Fig. 2. Variation in α, γ, ϵ and ζ of mvi-miR-9751.

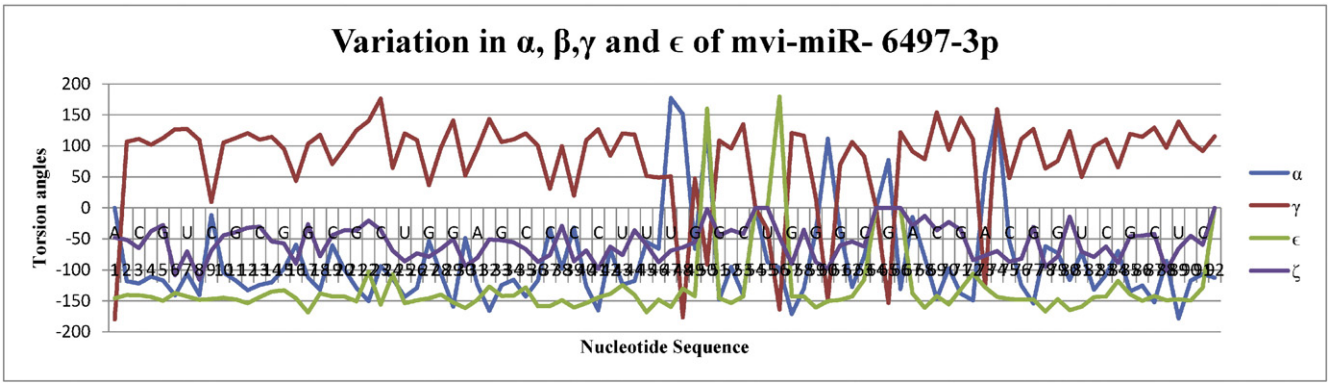

Fig. 3. Variation in α, γ, ϵ and ζ of mvi-miR-6497-3p.

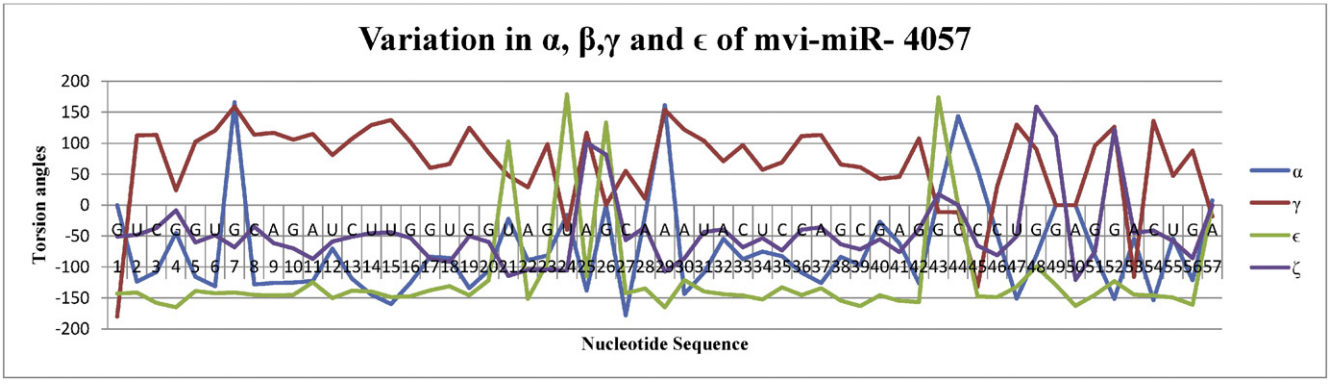

Fig. 4. Variation in α, γ, ϵ and ζ of mvi-miR-4057.

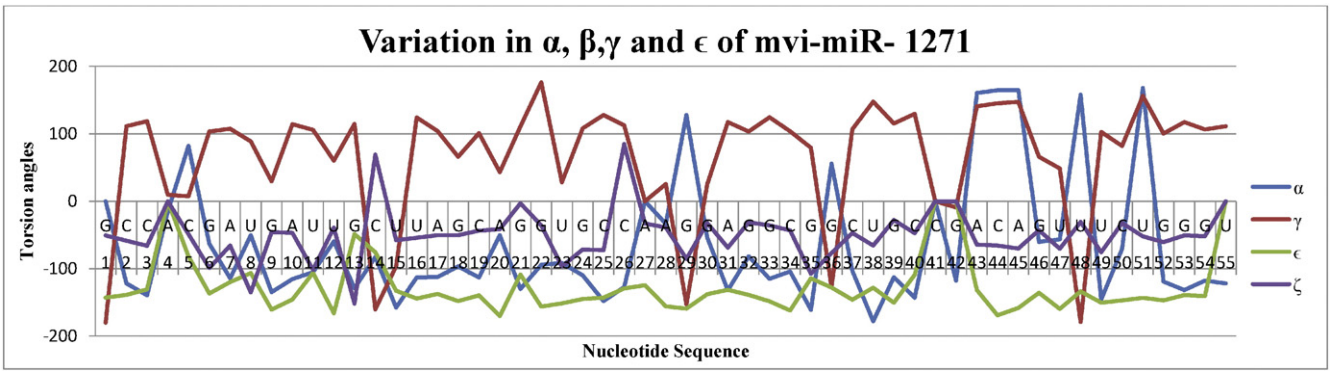

Fig. 5. Variation in α, γ, ϵ and ζ of mvi-miR-1271.

Table 4
α and γ torsion angle deviations in the predicted microRNAs.

miRNA	R	POS	ALPHA						GAMMA					
			MINIMUM			MAXIMUM			MINIMUM			MAXIMUM		
			BASE	ϕ	3plet	BASE	ϕ	3plet	BASE	ϕ	3plet	BASE	ϕ	3plet
mvi-miR -9751	S1	1–3	G2	−131.4	CGU	U3	−129.5	GUU	C1	−180	CGU	G2	144	CGU
		75–77	A75	−136.1	AAC	C76	−51.3	ACG	C76	64.6	ACG	A75	132	AAC
	S2	4–23	U12	−145.5	UUU	G16	86.6	GGU	G16	−142.5	GGU	U18	132.7	UUU
		54–74	A72	−178.8	AAA	A59	174.7	AAA	A70	−166.2	GAA	A59	166.1	AAA
	S3	26–34	U26	−144.1	GUU	G32	138.9	AGU	G32	−175.7	AGU	U27	130.7	UUA
		40–48	U46	−156.6	UUA	A48	−68.6	AAA	A48	66.2	AAA	U44	133.6	UUU
	IL1	24–25	G24	−144.7	AGG	G25	170.6	GGU	G24	124.6	AGG	G25	130.2	GGU
		49–53	A52	−173.7	AAU	U53	−39.8	AUU	A52	9.3	AAU	U53	162.9	AUU
	L	35–39	A38	−170.9	AAA	A36	62.3	AAA	A37	−166.4	AAA	A38	137	AAA
mvi-miR -6497-3p	S1	1–4	C3	−122.1	GCG	A1	0	AGC	A1	−180	AGC	C3	111.3	GCG
		91–92	G92	−112.9	CCG	C91	−107	CCG	C91	91.7	CCG	G92	115.3	CCG
	S2	5–25	G22	−150.5	GGC	C9	−11.6	GCG	C9	9.2	GCG	C23	176.1	GCC
		71–90	U89	−178.4	UUC	C74	156.5	ACC	A73	−127	GAC	C74	159.2	ACC
	S3	26–27	G26	−129.4	UGG	G27	−53.9	GGU	G27	36.7	GGU	G26	109.4	UGG
		69–70	C69	−146.6	UCC	C70	−97.5	CCG	C70	93.5	CCG	C69	154.1	UCC
	S4	33–39	C35	−143	CCA	C37	−34.2	ACG	C39	19.6	GCU	C35	120.1	CCA
		57–63	G57	−171.4	UGC	G60	111.7	GGG	G60	−151.2	GGG	G57	120.8	UGC
	S5	41–45	C41	−165.5	UCG	U45	−54.9	CUC	U45	51.4	CUC	C41	126.8	UCG
		50–54	G51	−148.1	GGA	G50	133.3	GGG	G50	−91.4	GGG	C53	135	ACG
	IL1	28–32	C32	−166.1	ACG	G30	−49.1	GGA	G30	52.1	GGA	C32	143.2	ACG
		64–68	A66	−131.1	GAA	G65	77.1	AGA	G65	−153.6	AGA	A66	121.9	GAA
	B	40				U40	−126.1	CUC				U40	109	CUC
		55–56	U56	−163.9	UUG	U55	−87.7	GUU	U56	−163.9	UUG	U55	−35.4	GUU
	L	46–49	C46	−65.9	UCU	U47	177.3	CUC	C48	−176.9	UCG	U47	50.7	CUC
mvi-miR -4057	S1	1–6	U6	−130.8	GUG	G16	0	GUC	G1	−180	GUC	U6	120.6	GUG
		53–57	C54	−153.4	ACU	A57	7.7	UGA	A53	−115.8	GAC	C54	136.2	ACU
	S2	8–30	C27	−178	GCA	A29	161.4	AAA	U24	−39.6	GUA	A29	153.8	AAA
		31–48	U47	−150.7	CUG	C44	143.7	GCC	C45	−132.1	CCC	U47	130.3	CUG
	IL1	7				G7	166.3	UGC				G7	159.2	UGC
		49–52	G52	−151.3	GAC	G49	0	GGA	G49	0	GGA	G52	126.6	GGA
mvi-miR -1271	S1	2–4	C3	−139.6	CCA	A4	−15.1	CAC	A4	9.4	CAC	C3	118.7	CCA
		51–53	G53	−131.7	GGG	U51	168.2	CUG	G52	100.3	UGG	U51	156.3	CUG
	S2	6–26	U15	−157.6	CUU	U8	−50.6	AUG	C14	−160.3	GCU	G22	176.1	GGU
		32–50	U38	−178	CUG	C44	164.5	ACA	U48	−179.1	UUU	U38	147.7	CUG
	EL	1				G1	0	GCC	G1	−180	GCC			
		54–55	U55	−122	GGU	G54	−118	GGU	G54	106.4	GGU	U55	111.3	GGU
	B	5				C5	82	ACG	C5	7.4	ACG			
	L	27–31	A31	−132.1	GAG	G29	127.8	AGG	G29	−153	AGG	A31	117.5	GAG

R—region; S—stem; IL—internal loop; B—bulge; EL—external loop; L—loop; POS—base position; ϕ—torsion angle value; 3plet—triplets. The coloured cells represent the torsion angle values that have deviated from the Klyne and Prelog cycle. Violet colour represents the highest deviation value and the orange colour represents the lowest deviation value.

sequence and these patterns were termed as "nucleotide triplets" (Table 6).

Also, when a bulge occurs in the stem region of a miRNA, it leads to variation in torsion angle (Kumar et al., 2012; Popenda et al., 2008).

Hence it is concluded that sequence composition can affect various structural motifs present in a pre-miRNA. This can help in understanding the sequence dependant modulations occurring in the cleaving of pri-miRNA by Drosha to synthesis pre-miRNA (Krol and Krzyzosiak,

Table 5
ϵ and ζ torsion angle deviations in the predicted microRNAs.

miRNA	R	POS	EPSILON						ZETA					
			MINIMUM			MAXIMUM			MINIMUM			MAXIMUM		
			BASE	ϕ	3plet	BASE	ϕ	3plet	BASE	ϕ	3plet	BASE	ϕ	3plet
mvi–miR –9751	S1	1–3	G2	−164.8	CGU	U3	−142.7	GUU	U3	−48	GUU	C1	−38	CGU
		75–77	G77	−142.7	CGU	A75	−126.1	AAC	G77	−51	CGU	C76	−43.2	ACG
	S2	4–23	U18	−159.6	UUU	A7	0	UAG	U17	−107.2	GUU	A7	0	UAG
		54–74	A71	−161.2	AAA	C68	55	CCG	C68	−128.7	CCG	A70	118.8	GAA
	S3	26–34	U34	−172.3	UUA	U27	−131.3	UUA	A29	−77.1	AAA	U34	130.7	UUA
		40–48	U42	−155.3	AUU	A48	−81.6	AAA	A40	−75.2	AAA	A48	126.1	AAA
	IL 1	24–25	G25	−146.2	GGU	G24	−116.1	AGG	G24	−85.6	AGG	G25	−44.2	GGU
		49–53	A51	−169.3	AAA	A52	0	AAU	A51	−42.3	AAA	A50	128.2	AAA
	L	35–39	A37	−171.7	AAA	A35	0	UAA	A37	−98.8	AAA	A36	87.1	AAA
mvi–miR –6497–3p	S1	1–4	A1	−146.1	AGC	G2	−140.9	AGC	C3	−65.1	GCG	G4	−37.6	GGA
		91–92	C91	−128.7	CCG	G92	0	CCG	C91	−59.5	CCG	G92	0	CCG
	S2	5–25	G17	−168.9	UGC	G22	−102.9	GGC	G8	−115.8	UGC	G22	−20.5	GGC
		71–90	C78	−167.2	GCG	G72	−105.9	GGA	U88	−101.3	CUU	U80	−14.1	GUU
	S3	26–27	G26	−149.7	UGG	G27	−146.1	GGU	G27	−79	GGU	G26	−73.7	UGG
		69–70	C70	−155.6	CCG	C69	−142.2	UCC	C69	−36.3	UCC	C70	−23	CCG
	S4	33–39	C39	−160.8	GCU	C35	−128.6	CCA	A36	−87.2	CAC	G38	−29.3	CGC
		57–63	G59	−161.1	CGG	C63	−116	GCA	G60	−98	GGG	C58	−35.4	GCG
	S5	41–45	U45	−168.5	CUC	U43	−124.8	GUC	C41	−98.5	UCG	C44	−36.4	UCU
		50–54	A52	−153.5	GAC	G50	160	GGG	G51	−44.4	GGA	G54	0	CGU
	IL1	28–32	G30	−161.6	GGA	C32	−127.1	ACG	G30	−94.3	GGA	G29	−50.3	UGG
		64–68	U68	−161.5	AUC	G65	0	AGA	A67	−29	AAU	G65	0	AGA
	B	40				U40	−153.9	CUC	U40	−68.7	CUC			
		55–56	U55	0	GUU	U56	179.6	UUG	U56	−47	UUG	U55	0	GUU
	L	46–49	U47	−159.9	CUC	C48	−130.5	UCG	C46	−87.7	UCU	G49	−55.3	CGG
mvi–miR –4057	S1	1–6	GA	−164.9	CGG	G5	−138.8	GGU	G5	−60.2	GGU	G4	−8.4	CGG
		53–57	G56	−161	UGA	A57	0	UGA	G56	−85.7	UGA	A57	0	UGA
	S2	8–30	A29	−165	AAA	U24	178.8	GUA	U21	−114.2	GUA	A25	100.8	UAG
		31–48	C39	−163.1	GCG	G43	174.3	GGC	C46	−81	CCU	G48	159.3	UGG
	IL1	7	G7	−141.3	UGC				G7	−68.1	UGC			
		49–52	A50	−162.6	GAG	G52	−122.8	GGA	A50	−120.5	GAG	G52	122.4	GGA
mvi–miR –1271	S1	2–4	C2	−138.9	GCC	A4	0	CAC	C3	−66	CCA	A4	0	CAC
		51–53	G52	−147.3	CUG	U55	0	GGU	G52	−60.7	UGG	G53	−50.9	GGG
	S2	6–26	A20	−170.4	CAG	G13	−48.8	UGC	G13	−151.8	UGC	C26	84.5	CCA
		32–50	C44	−169.4	ACA	C41	0	CCG	G35	−107.7	CGG	C41	0	CCG
	EL	1				G1	−140	GCC	G13	−50.9	GCC			
		54–55	G54	−140.8	GGU	U55	0	GGU	G54	−51.7	GGU	G53	−50.9	GGG
	B	5	C5	−81.9	ACG				C5	−48.9	ACG			
	L	27–31	G29	−159.3	AGG	A27	−124.8	CAA	G29	−85.4	AGG	G30	−32.3	GGA

R—region; S—stem; IL—internal loop; B—bulge; EL—external loop; L—loop; POS—base position; ϕ—torsion angle value; 3plet—triplets. The coloured cells represent the torsion angle values that have deviated from the Klyne and Prelog cycle. Violet colour represents the highest deviation value and the orange colour represents the lowest deviation value.

2004; Starega-Roslan et al., 2011). Studies have shown that the size, location and the distribution of terminal loops and internal loops can affect the cleavage by Dicer. Therefore a shift in the cleavage sites of the enzymes Drosha and Dicer can result in the formation of isomiRs (isoforms of mature miRNAs) (Fernandez-Valverde et al., 2010; Neilsen et al., 2012).

Table 6
Triplets and their deviation from torsion angles.

Triplets	Region	Alpha	Gamma	Epsilon	Zeta
C**C**G	Stem	**−97.5**	**93.5**	**−155.6**	**−23**
G**G**U	Stem	**86.6**	**−142.5**	**−157.2**	**−17.5**
G**U**U	Stem	**−131.4**	**119.0**	−122.8	**−91.8**
G**G**G	Stem	**133.3**	**−91.4**	**160.0**	**−2.1**
C**C**A	Stem	**−127.3**	**112.7**	−129.5	**84.5**
U**G**C	Internal loop	**166.3**	**159.2**	−141.3	−68.1
G**G**A	Internal loop	−49.1	52.1	**−161.6**	**−94.3**
A**A**A	Loop	**33.0**	**−166.4**	**−171.7**	**−98.8**
A**G**G	Loop	**127.8**	**−153.0**	**−159.3**	−85.4
A**C**G	Bulge	**82.0**	**7.4**	**−81.9**	**−48.9**

The outcome of this study can be implemented to investigate the effect of sequence variation in miRNAs and the resulting conformational changes observed during the binding of miRNAs to the RISC.

4. Conclusion

In the current study we identified thirteen putative miRNAs from *M. vitrata*. These miRNAs regulate mRNAs related to metamorphosis, cell signalling, transcription regulation, structural constituents, metabolism, and transmembrane transportation. miRNAs identified in the pest *M. vitrata* can be the initial step for an effective pest management programme.

Backbone torsion angles of precursor structures of mvi-miR-9751, mvi-miR-6497-3p, mvi-miR-4057 and mvi-miR-1271 show that sequence composition can influence the stem-loop hairpin structure of pre-miRNAs. The presence of certain nucleotide triplets in structural motifs of miRNA can show substantial variation in the torsion angle values in these regions and affects the location of binding of enzymes. This work could be extended to study the sequence dependant variation in torsion angle during the binding of miRNAs to enzymes and RISC.

References

Altschul, S.F., Madden, T.L., Schäffer, A.A., Zhang, J., Zhang, Z., Miller, W., et al., 1997. Gapped BLAST and PSI-BLAST: a new generation of protein database search programs. Nucleic Acids Res. 25, 3389–3402.

Ambros, V., 2012. MicroRNAs and developmental timing. Curr. Opin. Genet. Dev. 21, 511–517.

Arrigo, P., Mitra, C., Izzotti, A., 2012. Influence of pre-mirna compositional properties on RISC complex recruitment and target selection. 2012 7th Int. Symp. Heal. Informatics Bioinforma. IEEE, pp. 69–75.

Asante, S.K., Tamo, M., Jackai, L.E.N., 2001. Integrated management of cowpea insect pests using elite cultivars, date of planting and minimum insectcide application. Afr. Crop. Sci. J. 9, 655–665.

Asgari, S., 2011. Role of microRNAs in insect host–microorganism interactions. Front. Physiol. 2.

Asokan, R., Rebijith, K.B., Ranjitha, H.H., Roopa, H.K., Ramamurthy, V.V., 2013. Prediction and characterization of novel microRNAs from brown plant hopper, *Nilaparvata lugens* (Stål) (Hemiptera: Delphacidae). Entomol. Res. 43, 224–235.

Bartel, D.P., 2004. MicroRNAs : genomics, biogenesis, mechanism, and function. Cell 116, 281–297.

Brennecke, J., Stark, A., Russell, R.B., Cohen, S.M., 2005. Principles of microRNA-target recognition. PLoS Biol. 3, 0404–0418.

Cantó-Pastor, A., Mollá-Morales, A., Ernst, E., Dahl, W., Zhai, J., Yan, Y., et al., 2015. Efficient transformation and artificial miRNA gene silencing in Lemna minor. Plant Biol. (Stuttg.) 17, 59–65 (Suppl 1).

Dannon, E.a., Tamò, M., Van Huis, A., Dicke, M., 2010. Effects of volatiles from *Maruca vitrata* larvae and caterpillar-infested flowers of their host plant *Vigna unguiculata* on the foraging behavior of the parasitoid *Apanteles taragamae*. J. Chem. Ecol. 36, 1083–1091.

Das, A., 2010. Computational identification of conserved microRNAs and their targets in tea (*Camellia sinensis*). Am. J. Plant Sci. 1, 77–86.

Djuranovic, D., Lavery, R., Hartmann, B., 2002. α/γ transitions in the B-DNA backbone. Nucleic Acids Res. 30, 5398–5406.

Dos Santos, G., Schroeder, A.J., Goodman, J.L., Strelets, V.B., Crosby, M.A., Thurmond, J., et al., 2014. FlyBase: introduction of the *Drosophila melanogaster* Release 6 reference genome assembly and large-scale migration of genome annotations. Nucleic Acids Res. 43, 690–697.

Drummond, M.J., McCarthy, J.J., Sinha, M., Spratt, H.M., Volpi, E., Esser, K.a., et al., 2011. Aging and microRNA expression in human skeletal muscle: a microarray and bioinformatics analysis. Physiol. Genomics 43, 595–603.

Eichman, B.F., Ortiz-Lombardía, M., Aymamí, J., Coll, M., Ho, P.S., 2002. The inherent properties of DNA four-way junctions: comparing the crystal structures of holliday junctions. J. Mol. Biol. 320, 1037–1051.

Fernandez-Valverde, S.L., Taft, R.J., Mattick, J.S., 2010. Dynamic isomiR regulation in *Drosophila* development. RNA 16, 1881–1888.

Flores-jasso, C.F., Arenas-huertero, C., Reyes, J.L., Contreras-cubas, C., Covarrubias, A., Vaca, L., 2009. First step in pre-miRNAs processing by human Dicer. Acta Pharmacol. Sin. 30, 1177–1185.

Friedman, R.C., Farh, K.K., Burge, C.B., Bartel, D.P., 2009. Most mammalian mRNAs are conserved targets of microRNAs. Genome Res. 19, 92–105.

Ghosh, Z., Chakrabarti, J., Mallick, B., 2007. miRNomics—the bioinformatics of microRNA genes. Biochem. Biophys. Res. Commun. 363, 6–11.

Gong, M., Ma, J., Li, M., Zhou, M., Hock, J.M., Yu, X., 2012. MicroRNA-204 critically regulates carcinogenesis in malignant peripheral nerve sheath tumors. Neuro-Oncology 14, 1007–1017.

Gopali, J.B., Teggelli, R., Mannur, D.M., Yelshetty, S., 2010. Web-forming lepidopteran, *Maruca vitrata* (Geyer): an emerging and destructive pest in pigeonpea. Karnataka J. Agric. Sci. 23, 35–38.

Griffiths-Jones, S., Grocock, R.J., van Dongen, S., Bateman, A., Enright, A.J., 2006. miRBase: microRNA sequences, targets and gene nomenclature. Nucleic Acids Res. 34, 140–144.

Gu, J., Fu, H., Zhang, X., Li, Y., 2007. Identifications of conserved 7-mers in 3′-UTRs and microRNAs in *Drosophila*. BMC Bioinf. 8.

K. O, M.Z. A., 1989. Ecological studies on cowpea borers. I. Evaluation of yield loss of cowpea due to the pod borers. Annu Res Rev Gazipur (Bangladesh) (29 Jun).

Krol, J., Krzyzosiak, W.J., 2004. Structural aspects of microRNA biogenesis. IUBMB Life 56, 95–100.

Kumar, P., Lehmann, J., Libchaber, A., 2012. Kinetics of bulge bases in small rnas and the effect of pressure on it. PLoS One 7, 2–9.

Lavery, R., Moakher, M., Maddocks, J.H., Petkeviciute, D., Zakrzewska, K., 2009. Conformational analysis of nucleic acids revisited: Curves+. Nucleic Acids Res. 37, 5917–5929.

Lee, Y., Ahn, C., Han, J., Choi, H., Kim, J., Yim, J., et al., 2003. The nuclear RNase III Drosha initiates microRNA processing. Nature 425, 415–419.

Lewis, B.P., Shih, I., Jones-rhoades, M.W., Bartel, D.P., Burge, C.B., 2003. Prediction of mammalian microRNA targets. Cell 115, 787–798.

Liao, C.T., Lin, C.S., 2000. Occurrence of the legume pod borer, *Maruca testulalis* Geyer (Lepidoptera: Pyralidae) on cowpea (*Vigna unguiculata* Walp) and its insecticides application trial. Plant Prot. Bull. 42, 213–222.

Mehinto, J.T., Atachi, P., Kobi, O., Kpindou, D., Tamò, M., 2014. Pathogenecity of entomopathogenic fungi *Metarhizium anisopliae* and *Beauveria bassiana* on larvae of the legume pod borer *Maruca vitrata* (Lepidoptera : Crambidae). ARPN J. Agric. Biol. Sci. 9, 55–64.

Neilsen, C.T., Goodall, G.J., Bracken, C.P., 2012. IsomiRs—the overlooked repertoire in the dynamic microRNAome. Trends Genet. 28, 544–549.

Parisien, M., Major, F., 2008. The MC-Fold and MC-Sym pipeline infers RNA structure from sequence data. Nature 452, 51–55.

Popenda, L., Adamiak, R.W., Gdaniec, Z., 2008. Bulged adenosine influence on the RNA duplex conformation in solution. Biochemistry 47, 5059–5067.

Saenger, W., 1983. Principles of Nucleic Acid Structures. Springer, New York.

Sanli, D., Keskin, O., Gursoy, A., Erman, B., 2011. Structural cooperativity in histone H3 tail modifications. Protein Sci. 20, 1982–1990.

Schneider, B., Morávek, Z., Berman, H.M., 2004. RNA conformational classes. Nucleic Acids Res. 32, 1666–1677.

Sharma, H.C., 1998. Bionomics, host plant resistance, and management of the legume pod borer, *Maruca vitrata* — a review. Crop. Prot. 17, 373–386.

Shivdasani, R.A., 2006. MicroRNAs: regulators of gene expression and cell differentiation. Blood 108, 3646–3653.

Starega-Roslan, J., Koscianska, E., Kozlowski, P., Krzyzosiak, W.J., 2011. The role of the precursor structure in the biogenesis of microRNA. Cell. Mol. Life Sci. 68, 2859–2871.

Svozil, D., Kalina, J., Omelka, M., Schneider, B., 2008. DNA conformations and their sequence preferences. Nucleic Acids Res. 36, 3690–3706.

Temiz, N.A., Donohue, D.E., Bacolla, A., Luke, B.T., Collins, J.R., 2012. The role of methylation in the intrinsic dynamics of B- and Z-DNA. PLoS One 7, 1–9.

Tiwari, M., Sharma, D., Trivedi, P.K., 2014. Artificial microRNA mediated gene silencing in plants: progress and perspectives. Plant Mol. Biol. 86, 1–18.

Zahid, M.A., Islam, M.M., Begum, M.R., 2008. Determination of economic injury levels of *Maruca vitrata* in mungbean. J. Agric. Rural. Dev. 6, 91–97.

Zhang, B., Pan, X., Anderson, T.A., 2006. Identification of 188 conserved maize microRNAs and their targets. FEBS Lett. 580, 3753–3762.

Zuker, M., 2003. Mfold web server for nucleic acid folding and hybridization prediction. Nucleic Acids Res. 31, 3406–3415.